Pattern dynamics associated with on-off convection in a one-dimensional system

Hidenori Ohara* and Hirokazu Fujisaka†
Department of Applied Analysis and Complex Dynamical Systems, Graduate School of Informatics, Kyoto University, Kyoto 606-8501, Japan

Katsuya Ouchi‡
Kobe Design University, 8-1-1 Gakuennishi-Machi, Nishi-ku, Kobe 651-2196, Japan
(Received 16 October 2002; published 29 April 2003)

A numerical and theoretical analysis of the phenomenologically constructed nonlinear stochastic model of on-off intermittency experimentally observed by John *et al.* in the electrohydrodynamic convection in nematic liquid crystal under applied dichotomous electric field is carried out. The model has the structure of the one-dimensional Swift-Hohenberg equation with a fluctuating threshold which represents an applied electric field and either with or without additive noise which corresponds to thermal noise. It is found that the fundamental statistics of pattern dynamics without additive noise agree with those experimentally observed, and also with those reported previously in two-dimensional system. In contrast to that the presence of multiplicative noise generates an intermittent evolution of pattern intensity, whose statistics are in agreement with those of on-off intermittency so far known, the additive noise gives rise to the change of position of the convective pattern. It is found that the temporal evolution of the phase suitably introduced to describe the global convective pattern also shows an intermittent evolution. Its statistics are studied in a detailed way with numerical simulation and stochastic analysis. The comparison of these results turn out to be in good agreement with each other.

DOI: 10.1103/PhysRevE.67.046223 PACS number(s): 05.45.−a, 47.54.+r, 61.30.−v, 05.40.−a

I. INTRODUCTION

Intermittency spatially or temporally observed is a ubiquitous phenomenon in nonlinear systems. The small-scale dynamics in hydrodynamic turbulence is the most famous example. An intermittency is also often observed in dynamical systems which show chaotic motions. For example, the intermittency known as modulational intermittency or on-off intermittency occurs when a synchronized chaos in a coupled chaotic oscillator system undergoes the instability as the control parameter is changed [1–3]. On-off intermittency has been often studied in dynamical systems with a small number of degrees of freedom [4–6]. Several years ago, the observation of the intermittency was first reported experimentally in the system with a large number of degrees of freedom, e.g., in the spin wave instability [7].

It is known that the on-off intermittency has the three characteristic statistics [4]: (i) the probability density $P(l)$ for $l(t)$, the magnitude of the deviation from the particular chaotic submanifold, asymptotically obeys a power law with exponent $-1+\eta$, where η is a small positive value, (ii) the spectral intensity of time series $\{l(t)\}$ exhibits a power law with the exponent $-1/2$ in a low frequency region, and (iii) the probability density $Q(\tau)$ for the laminar duration τ, where the laminar state stands for that being close to the particular chaotic submanifold, asymptotically takes a power law with the exponent $-3/2$ for a wide range of τ. The characteristics (i) and (ii) are explained by a nonlinear multiplicative stochastic model for the time evolution of $l(t)$. In fact, according to the multiplicative noise model, the exponent η is determined as

$$\eta=\frac{\lambda}{\Gamma_f}, \tag{1}$$

where λ (>0) represents the deviation of the external control parameter from its critical value and Γ_f is the intensity of the modulational noise of the so-called local transverse expansion rate. Third characteristic statistics (iii) is simply derived by the theory of first passage time problem of Brownian motion of the linearized multiplicative stochastic model.

The electrohydrodynamic convection (EC) is one of the most famous examples in nonequiliblium systems observed in liquid crystal system [8]. In the nematic liquid crystal system, EC caused by the electrohydrodynamic instability (EHD) under an electric field is quite famous. So far, studies on EC have been mainly carried out by applying temporally periodic electric field [9]. On the other hand, several works on EC under the application of stochastic electric field were reported [10–14]. Recently, Behn, Lange, and John predicted that even if the pure dichotomous noise is applied, the onset of the EC would be observed as the amplitude of noise is increased [11]. This prediction was recently experimentally proved by John, Stannarius, and Behn (JSB) [12]. In addition, they reported that the intermittency is observed in association with the onset of EC, and showed that it quite resembles to the signature of on-off intermittency, observing the laminar duration distribution, where the laminar state implies the planar alignment of directors along the electrode planes [12]. Furthermore, very recently, they reported that the probability density of the pattern intensity and the spec-

*Electronic address: ohara@acs.i.kyoto-u.ac.jp
†Electronic address: fujisaka@i.kyoto-u.ac.jp
‡Electronic address: ouchi@kobe-du.ac.jp

tral intensity of time series of the pattern intensity are also same as those of on-off intermittency [13,14].

In a previous paper, in order to explain JSB's result in Ref. [12], we proposed a phenomenological nonlinear stochastic model for EC under the stochastic electric field [15]. The model has the structure of the Swift-Hohenberg equation with the noise-modulated growth rate. In the study using this equation in the two-dimensional (2D) system [15], we reported that the numerical integration shows intermittent emergence of convective pattern and that its statistics are same as those known for on-off intermittency. However, although the pattern intensity changes intermittently in the course of time, no global pattern change is observed. Noting the existence of thermal noise, we added the additive noise term in the our model equation. It was found that the introduction of the additive noise makes the pattern form change. This implies that the effect of thermal noise plays the global pattern dynamics in the present situation.

The fundamental aim of the present paper is to study the details of the statistical dynamics of the phenomenological model in the 1D system both numerically and theoretically. Particularly, we will study the statistics of a phase variable associated with the intermittent change of convective pattern. The present paper is organized as follows. In Sec. II, we propose a phenomenological stochastic model of EC under the stochastic electric field. A few characteristics of the model are pointed out. Numerical results on the stochastic dynamics of convective pattern dynamics are given in Sec. III. The onset of intermittent emergence of convective pattern intensity will be observed. Furthermore, it is shown that in contrast to that the random modulation in the threshold causes the change of pattern intensity, thermal noise makes the pattern itself change. Theoretical analysis of our model is developed in Sec. IV. We propose the statistics of the phase variable relevant to convective pattern and compare the theory with the numerical simulations. In Sec. V, we discuss the phase diffusion of the most unstable mode. The mean square displacement of the phase is calculated analytically and is compared to the numerical simulation. We give conclusion and remarks in Sec. VI.

II. PHENOMENOLOGICAL MODEL FOR EC INDUCED BY APPLIED STOCHASTIC FIELD

Although thermal convection of neutral fluid has often been studied both experimentally and theoretically [8,16,17], it is quite difficult to study EC by starting with the fundamental equations of motion for EHD because they are quite complicated. Near the convection threshold, there appear two kinds of modes; critical and noncritical. The former is directly relevant to the formation of convective pattern and the latter is stably slaved to the critical mode. Adiabatically eliminating noncritical modes, Swift and Hohenberg (SH) derived the amplitude equation,

$$\frac{\partial w(\mathbf{r},t)}{\partial t}=[\lambda-(\nabla^2+k_c^2)^2]w(\mathbf{r},t)-w^3(\mathbf{r},t), \tag{2}$$

near the onset of convective pattern in thermal convection in neutral fluid [8,16,17]. Here, $w(\mathbf{r},t)$ is the vertical component of macroscopic local velocity of fluid at position $\mathbf{r}$ at time t, λ is the deviation of the Rayleigh number R from its critical value R_c, i.e., $\lambda=R-R_c$, k_c being the wave number of the most unstable mode.

In this paper, we phenomenologically extend the SH equation, adding multiplicative noise and additive noise, i.e.,

$$\frac{\partial w(\mathbf{r},t)}{\partial t}=[\lambda+f(t)-(\nabla^2+k_c^2)^2]w(\mathbf{r},t)-w^3(\mathbf{r},t)+g(\mathbf{r},t). \tag{3}$$

In the experimental situation of JSB [12], $w(\mathbf{r},t)$ is the gradient of the angle between the local director and the electrode plates, and λ is the mean deviation from its critical value. The k_c is the wave number of the linearly most unstable mode. The $f(t)$ is the applied spatially uniform modulation noise and,

$$\Gamma_f=\int_0^\infty \langle f(t)f(t')\rangle dt, \tag{4}$$

is the intensity of the threshold modulation, where the angular brackets stand for the ensemble average. The $g(\mathbf{r},t)$ represents thermal noise and is assumed to be Gaussian-white noise, i.e.,

$$\langle g(\mathbf{r},t)\rangle=0, \quad \langle g(\mathbf{r},t)g(\mathbf{r}',t')\rangle=2\varepsilon\,\delta(\mathbf{r}-\mathbf{r}')\,\delta(t-t'). \tag{5}$$

One should note that $\Gamma_f \gg \varepsilon$ because the external stochastic field is more crucial than the thermal noise.

Equation (3) always has a quiescent state $w(\mathbf{r},t)=0$ for any $\mathbf{r}$ and t, which corresponds to the complete planar alignment of directors to the electrodes, provided $g(\mathbf{r},t)$ is absent. The linear stability of this state is examined with the $\mathbf{k}$-mode growth rate,

$$\lambda_k\equiv\lambda-(k^2-k_c^2)^2 \quad (k=|\mathbf{k}|). \tag{6}$$

If $\lambda<0$, there exists no unstable mode and the spatial pattern eventually decays into the planar state. On the other hand, if $\lambda>0$, the planar state is unstable for modes with wave numbers around k_c, and this situation leads to the emergence of convective pattern.

III. NUMERICAL SIMULATIONS AND RESULTS

In the present paper, we consider the 1D system with the system size L. The pattern intensity at time t is measured by the quantity

$$l(t)\equiv\left\{\frac{1}{L}\int_0^L [w(x,t)]^2dx\right\}^{1/2}. \tag{7}$$

If $l(t)=0$, no convective pattern is present at time t.

The applied spatially uniform noise $f(t)$ is assumed to be generated by the Ornstein-Uhlenbeck process,

$$\frac{df(t)}{dt}=-\gamma f(t)+R(t), \tag{8}$$

where $R(t)$ is the Gaussian-white noise with the statistics,

$$\langle R(t)\rangle = 0, \quad \langle R(t)R(t')\rangle = 2D\delta(t-t'), \tag{9}$$

with positive values γ and D. The statistics of $f(t)$ is therefore Gaussian and has the correlation function

$$\langle f(t)f(t')\rangle = \gamma\Gamma_f e^{-\gamma|t-t'|}, \tag{10}$$

and the noise intensity Γ_f of $f(t)$ is related γ and D via

$$\Gamma_f = \frac{D}{\gamma^2}. \tag{11}$$

Hereafter, we numerically and theoretically investigate Eq. (3) without thermal noise (model *A*) and with thermal noise (model *B*). Numerical simulations are carried out with the use of the Euler scheme for stochastic differential equations interpreted in the Stratonovich sense [18,19]. The time step for numerical integration was set as $\Delta t = 5\times 10^{-4}$. We integrate the scalar field on 256 lattice points with the periodic boundary condition. The parameter values were set to be $k_c = 1$ and $L = 32\pi$. The initial condition was chosen in such a way that initially $w(x,0)$ at each lattice point is randomly distributed with the mean zero and the variance 10^{-5}.

A. Model *A*

We first consider the case without thermal noise. The governing equation is written as

$$\frac{\partial w(x,t)}{\partial t} = [\lambda + f(t) - (\nabla^2 + k_c^2)^2]w(x,t) - w^3(x,t). \tag{12}$$

We carry out the numerical integration of Eq. (12) for several different values of λ, D, and γ with the quasispectral method. Figure 1 shows the temporal evolution of spatial pattern and $\{l(t)\}$ obtained by numerically solving Eq. (12). One clearly observes that the temporal evolution of $l(t)$ and the spatial pattern show intermittency composed of laminar regions where no apparent pattern change are observed and burst regions where the spatial pattern with the wave number k_c are generated. The temporal evolution of $l(t)$ is quite similar to that of the so-called on-off intermittency. There exists no change of position of the pattern form.

Numerical results with the statistical laws of on-off intermittency are compared. Calculating the exponent $\eta = \lambda/\Gamma_f$ by Eq. (1), we theoretically get probability densities for $l(t)$ with the exponent estimated from several values of λ, D, and γ. As shown in Fig. 2, one finds a good agreement with numerical results.

The second characteristic of on-off intermittency is the $\omega^{-1/2}$ law in the low frequency region of the power spectrum is shown in Fig. 3. However, the power law $\omega^{-1/2}$ is not clearly observed for all parameters λ, D, and γ used in the present numerical simulation. The region where the asymptotic law $I(\omega)\propto\omega^{-1/2}$ is observed is estimated as $\lambda^2/\Gamma_f \ll \omega \ll \Gamma_f$ [6]. In the present simulation, however, the ratio Γ_f/λ is not sufficiently large for parameter values of λ, D, and γ which we used. This is the reason why the power law $\omega^{-1/2}$ is not so clearly observed. It is worth noting that for a large ω region, the power law $\omega^{-3/2}$ is rather observed in a wide range. This fact may suggest that the on-off intermittency can exhibit another characteristic observed is the power spectrum in an intermediate frequency range, or may be derived from our model. However, there exists no theoretical explanation on this power law.

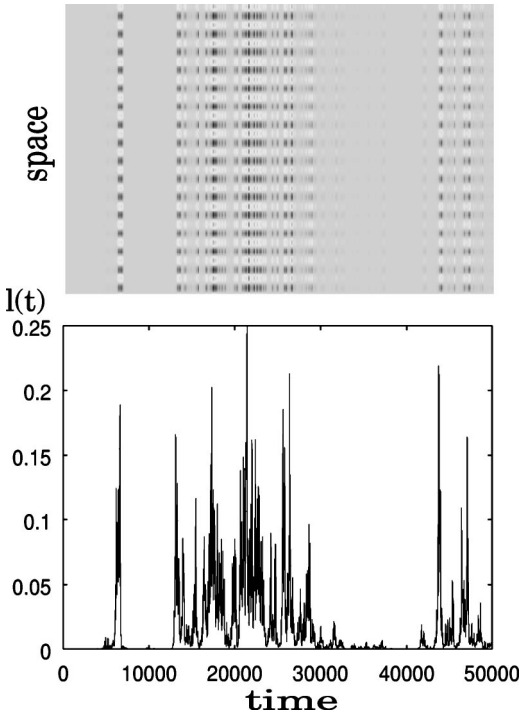

FIG. 1. Simultaneous plots of evolutions of pattern (upper) and time series of $l(t)$ (lower) for $\lambda = 0.001$, $D = 10$, $\gamma = 50$. Dark region corresponds to positive values of $w(x,t)$, gray region to values close to zero, and white region to negative values. One observes that when a pattern is generated, $l(t)$ takes a nonvanishing value. The pattern generation is intermittent.

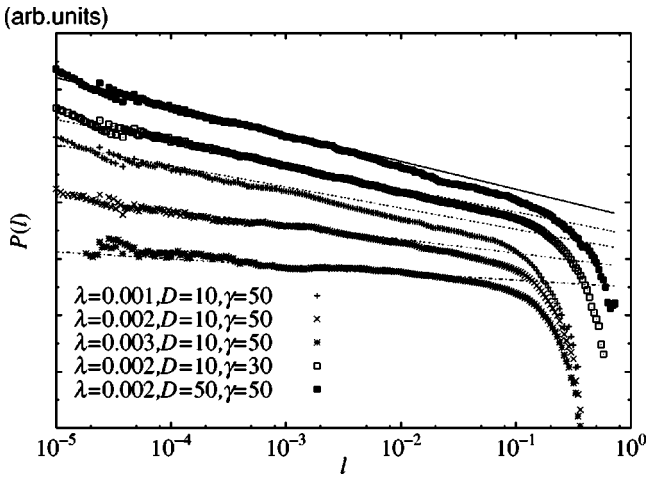

FIG. 2. Probability densities $P(l)$ of $l(t)$ for various choices of parameters. Symbols are the results of numerical simulation for the model (12) in comparison with the theoretical results $P(l)\propto l^{-1+\eta}$ (lines).

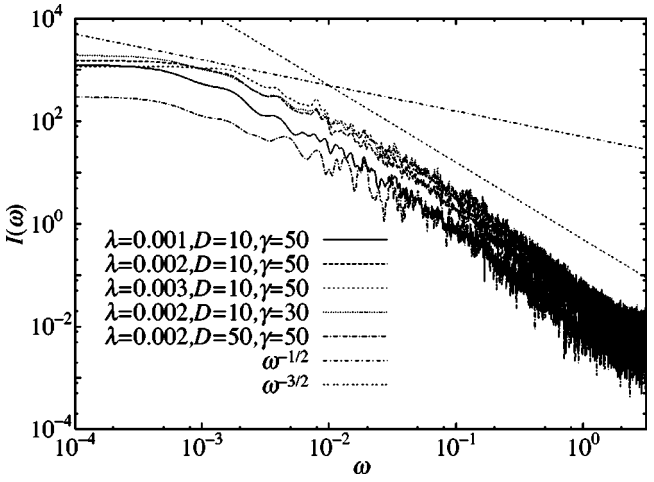

FIG. 3. Spectral intensities of time series $l(t)$ for various choices of parameters. Shown are the results of numerical simulation using the model (12) in comparison with $\omega^{-1/2}$ and $\omega^{-3/2}$.

The statistics of laminar duration was studied with the laminar duration distribution by constructing the histogram of laminar durations. Here, the laminar duration is defined as the duration where l is below a threshold l_{th} suitably chosen, separating laminar ($l<l_{th}$) and burst ($l>l_{th}$) states. In Fig. 4, the laminar duration distribution obtained from the numerical results is given. One finds that the observed laminar duration distribution clearly shows the power law $\tau^{-3/2}$ which is one of the most well-known characteristics of on-off intermittency [4]. Here, l_{th} was chosen as 0.005. We confirmed that the exponent 3/2 does not depend on the choice of l_{th} as far as it is sufficiently small.

We thus observed the intermittent emergence of convective pattern associated with the instability of the planar alignment with $w=0$ under the application of multiplicative noise in the threshold. The intermittency has statistics same as those of on-off intermittency, and agrees with the observation by John *et al.* [11–13]. In this sense, in the previous paper, the phenomenon was termed on-off convection [15].

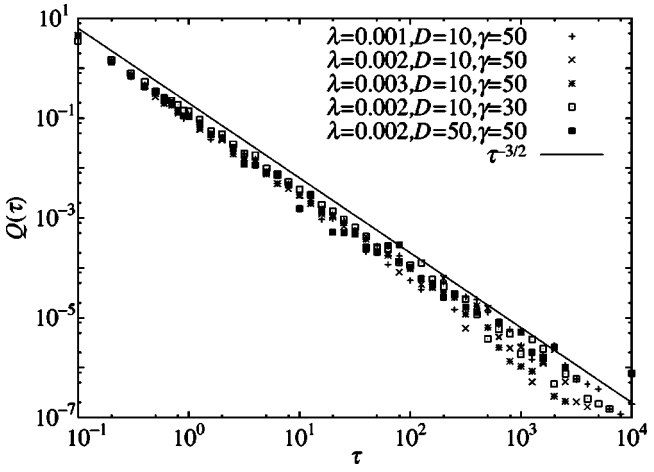

FIG. 4. Laminar duration distributions $Q(\tau)$ for various choices of parameters. Symbols are the results of numerical simulation using the model (12) in comparison with $\tau^{-3/2}$ (line).

B. Model *B*

As shown in the preceding section, the form of convective pattern does not change for the dynamical equation without thermal noise. In a real system, the temporal evolution is affected by thermal noise. Hereafter, we investigate its effect on the temporal evolution of convective pattern. Parameters are set as $\lambda=0.002$, $D=100$, and $\gamma=50$. With the periodic boundary condition, we carry out the mode expansion of $w(x,t)$ as

$$w(x,t)=\sum_{n=-\infty}^{\infty}\hat{w}_n e^{ik_n x},\quad k_n=nk_1,\quad k_1=\frac{2\pi}{L}. \tag{13}$$

Substituting the expansion (13) into Eq. (3), we get the equations of motion for $\hat{w}_n$ as

$$\frac{d\hat{w}_n(t)}{dt}=[\lambda_{k_n}+f(t)]\hat{w}_n(t)-\sum_{n_1+n_2+n_3=n}\hat{w}_{n_1}\hat{w}_{n_2}\hat{w}_{n_3}+\hat{g}_n(t). \tag{14}$$

Here, $\hat{g}_n(t)$ $[=\hat{g}^*_{-n}(t)]$ is the Fourier coefficient for the k_n mode and is defined as

$$\hat{g}_n(t)=\frac{1}{L}\int_0^L g(x,t)e^{-ik_n x}dx. \tag{15}$$

The statistics (5) implies

$$\langle\hat{g}_n(t)\rangle=0,\quad \langle\hat{g}_n(t)\hat{g}_{n'}(t')\rangle=2\bar{\varepsilon}\delta_{n,-n'}\delta(t-t'), \tag{16}$$

where $\bar{\varepsilon}=\varepsilon/L$. Since the only mode with the wave number k_c is unstable slightly above $\lambda=0$, truncating stable modes except for the modes with the wave numbers k_c, $k_c\pm k_1$, and $k_c\pm 2k_1$, we get the equations of motion for $\hat{w}_n$ with the wave numbers k_c, $k_c\pm k_1$, and $k_c\pm 2k_1$. Thus, the governing equations for the numerical simulation are given as

$$\frac{d\hat{w}_{n_c}(t)}{dt}=[\lambda+f(t)]\hat{w}_{n_c}(t)-N_{n_c}(t)+\hat{g}_{n_c}(t), \tag{17}$$

$$\frac{d\hat{w}_{n_c\pm1}(t)}{dt}=\{\lambda-[(n_c\pm1)^2-n_c^2]^2k_1^4+f(t)\}\hat{w}_{n_c\pm1}(t)-N_{n_c\pm1}(t)+\hat{g}_{n_c\pm1}(t), \tag{18}$$

$$\frac{d\hat{w}_{n_c\pm2}(t)}{dt}=\{\lambda-[(n_c\pm2)^2-n_c^2]^2k_1^4+f(t)\}\hat{w}_{n_c\pm2}(t)-N_{n_c\pm2}(t)+\hat{g}_{n_c\pm2}(t), \tag{19}$$

where $n_c=k_c/k_1$, and $N_{n_c}(t)$, $N_{n_c\pm1}(t)$, and $N_{n_c\pm2}$ are nonlinear terms of each mode. We will carry out numerical simulation for several different values of the intensity ε of thermal noise.

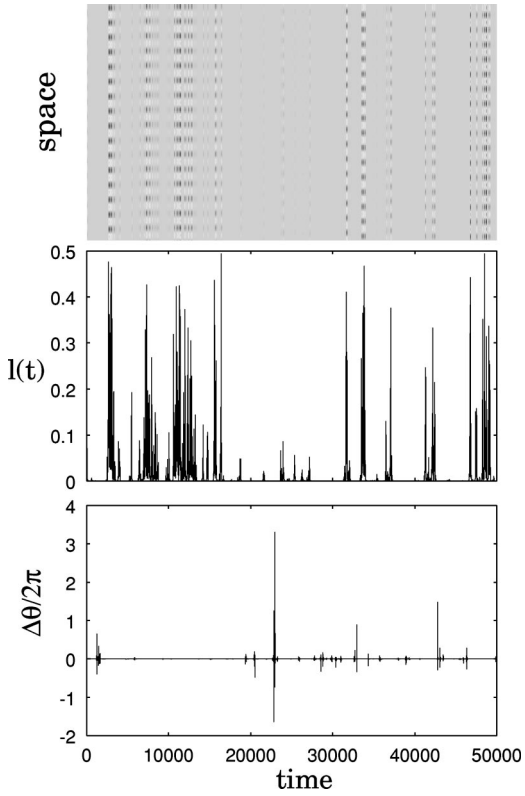

FIG. 5. Numerical results of pattern evolution (upper), its corresponding time series of the pattern intensity $l(t)$ (middle) and the phase change of $\hat{w}_{n_c}(t)$ per unit time for the k_c mode (lower) for $\lambda=0.002$, $D=100$, $\gamma=50$, and $\varepsilon=10^{-14}$. The dark regions correspond to positive values of $w(x,t)$, the gray regions to values close to zero, and the white region to negative values.

Here, we define the phase $\theta(t)$ by

$$\hat{w}_{n_c}(t)\equiv r(t)\exp[i\theta(t)] \quad (r(t)\equiv|\hat{w}_{n_c}(t)|).$$

It is easy to understand that the phase is clearly connected with the spatial form of $w(x,t)$. In order to observe the statistics of the temporal evolution of the phase changes for the k_c mode, we define $\Delta\theta$ as the phase change of the k_c mode per time step Δt. Figure 5 shows the temporal evolution of the spatial pattern, the pattern intensity $l(t)$, and the phase change $\Delta\theta$ per unit time for the k_c mode obtained by numerically integrating Eqs. (17), (18), and (19).

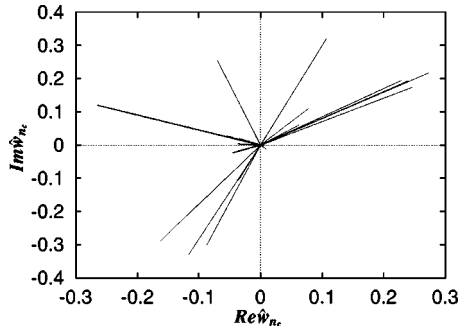

FIG. 6. Plot of a trajectory of the k_c mode on the complex $\hat{w}_{n_c}(t)$ plane. Parameter values are same as in Fig. 5. One observes no phase change when $|\hat{w}_{n_c}(t)|$ is not small enough.

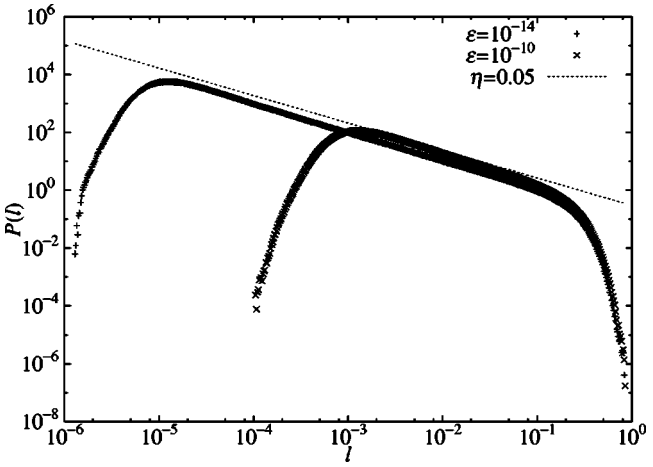

FIG. 7. Probability density $P(l)$ of $l(t)$. Shown are the results of numerical simulation with model *B* (symbols) and the theoretical result $P(l)\propto l^{-1+\eta}$ (line). The theoretical curve is obtained for $\lambda=0.002$, $D=100$, $\gamma=50$, and, therefore, $\eta=0.05$.

It is worth to note that the time evolution of $l(t)$ is connected to that obtained for model *A*. This is same as in Fig. 1. In addition, one observes that when the pattern form changes, the time series of the phase change $\Delta\theta$ shows a prominent intermittent characteristic. Figure 6 shows the trajectories for the k_c mode on the complex $\hat{w}_{n_c}(t)$ plane. It is observed that the phase does not change when the amplitude $r(t)$ is large and it suddenly changes due to thermal noise when the amplitude almost vanishes.

Figures 7, 8, and 9 are the statistics of the temporal evolution of $l(t)$, i.e., its probability density, the power spectrum and the laminar duration distribution under the effect of additive noise. The numerical results are almost same as for model *A* because of a weak intensity of thermal noise. However, one should note that the probability density $P(l)$ for

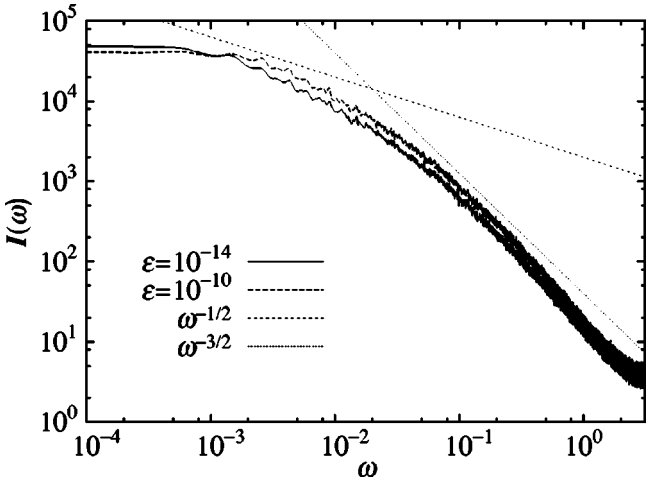

FIG. 8. The spectral intensity of time series $l(t)$ $I(\omega)$. Shown are the results of numerical simulation with model *B* in comparison with the power laws $\omega^{-1/2}$ and $\omega^{-3/2}$.

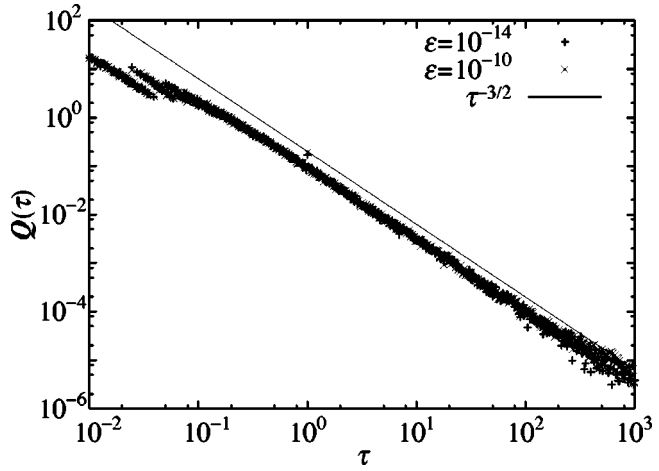

FIG. 9. The laminar duration distribution $Q(\tau)$. Shown are the results of numerical simulation with model *B* (symbols) in comparison with $\tau^{-3/2}$ (line).

$l(t)$ does not obey the asymptotic power law $l^{-1+\eta}$ in a small l region as ε is increased. This is because that the thermal noise smears the singularity of the statistics at $l(t)=0$. Figure 10 shows the probability density for the phase change $\Delta\theta$. The numerical result suggests the possibility of a new statistics associated with the intermittent change of convective pattern. The details of the statistics will be theoretically studied in the following section.

IV. THEORETICAL RESULTS FOR MODEL *B*

A. Linear analysis

With the mode expansion Eq. (14) of $w(x,t)$, the on-off variable $l(t)$ defined in Eq. (7) is evaluated as $l(t) \approx [\Sigma_n |\hat{w}_n(t)|^2]^{1/2}$. Here, we examine the linear stability of $\hat{w}_n(t)=0$, i.e., nonconvective state, for each mode. By dropping out the nonlinear terms in Eq. (14) and approximating

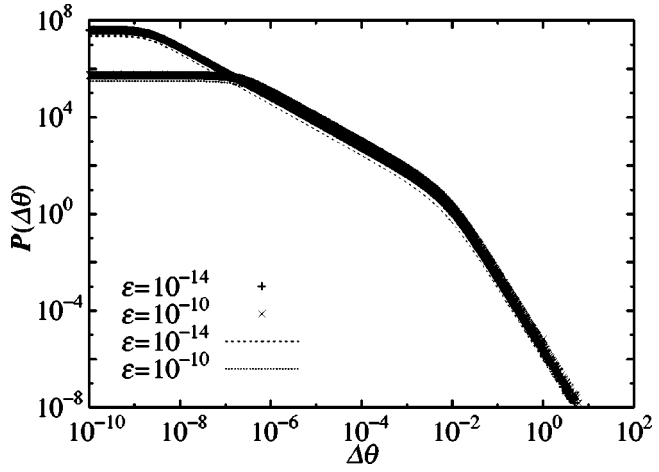

FIG. 10. Probability density $P(\Delta\theta)$ of the phase change $\Delta\theta(t)$ for the time difference $\Delta t=0.0005$. The results of numerical simulation (symbols) are compared with the theoretical result Eq. (39) (lines).

that $f(t)$ is Gaussian white, the ensemble average of $|\hat{w}_n(t)|^2$ for the stationary state is given as

$$\langle|\hat{w}_n(t)|^2\rangle \sim \langle|\hat{w}_n(0)|^2\rangle e^{2(\lambda_{k_n}+\Gamma_f)t} + \frac{\overline{\varepsilon}}{\lambda_{k_n}+\Gamma_f}[e^{2(\lambda_{k_n}+\Gamma_f)t}-1]. \tag{20}$$

Thus, the modes with $\lambda_{k_n}+\Gamma_f<0$ are stable, and the modes with $\lambda_{k_n}+\Gamma_f>0$ are unstable. Moreover, if ε is increased, we get the estimation $\langle|\hat{w}_n(t)|^2\rangle \sim \overline{\varepsilon}/|\lambda_{k_n}+\Gamma_f|$ in the laminar state so that it becomes harder for $l(t)$ to vanish in the laminar state. This fact implies that if the intensity of thermal noise is increased, the pattern will not disappear completely.

B. Statistics of $l(t)$ and phase changes

The statistics of $l(t)$ is theoretically discussed as follows. Suppose that only the mode with the wave number k_c is unstable, and other modes are $\hat{w}_n(t)\simeq 0$ $(n\neq \pm k_c/k_1)$ in the stationary state. Thus, the system behavior is determined by the k_c mode. The substitution of $\hat{w}_n(t)\simeq 0$ except for $n_c(\equiv k_c/k_1)$ into Eq. (14) leads to

$$\frac{d\hat{w}_{n_c}(t)}{dt} = [\lambda+f(t)]\hat{w}_{n_c}(t) - 3|\hat{w}_{n_c}(t)|^2\hat{w}_{n_c}(t) + \hat{g}_{n_c}(t). \tag{21}$$

Using $\hat{w}_{n_c}(t)\equiv r(t)\exp[i\theta(t)]$, we get the equations of motion for $r(t)$ and $\theta(t)$,

$$\frac{dr(t)}{dt} = [\lambda+f(t)]r(t) - 3r(t)^3 + g_r(t), \tag{22}$$

$$\frac{d\theta(t)}{dt} = \frac{1}{r(t)}g_\theta(t). \tag{23}$$

Here, we assumed that $g_r(t)$ and $g_\theta(t)$ are statistically independent Gaussian-white noises, i.e., $\langle g_r(t)g_\theta(t')\rangle=0$ and

$$\langle g_r(t)\rangle = 0, \quad \langle g_r(t)g_r(t')\rangle = \overline{\varepsilon}\,\delta(t-t'), \tag{24}$$

$$\langle g_\theta(t)\rangle = 0, \quad \langle g_\theta(t)g_\theta(t')\rangle = \overline{\varepsilon}\,\delta(t-t'). \tag{25}$$

Equation (23) immediately shows that there exists no temporal evolution of $\theta(t)$ if thermal noise is absent, i.e., no change of the pattern form is observed if thermal noise is absent (Fig. 1).

The Fokker-Planck equation for the joint probability density $Q(r,\theta,t)$ of $r(t)$ and $\theta(t)$ can be written as [20–22]

$$\frac{\partial Q(r,\theta,t)}{\partial t} = -\frac{\partial}{\partial r}\{[(\lambda+\Gamma_{\rm eff})r-3r^3]Q(r,\theta,t)\} + \frac{\partial^2}{\partial r^2}\left[\left(\frac{\bar{\varepsilon}}{2}+\Gamma_{\rm eff}r^2\right)Q(r,\theta,t)\right] + \frac{\bar{\varepsilon}}{2r^2}\frac{\partial^2 Q(r,\theta,t)}{\partial\theta^2}, \tag{26}$$

where we used the Markov approximation. $\Gamma_{\rm eff}$ is the effective colored-noise strength given by

$$\Gamma_{\rm eff} = \frac{\Gamma_f}{1+6\gamma^{-1}\langle r^2\rangle}, \tag{27}$$

(see Refs. [20,21]). Here, we defined

$$P(r,t) \equiv \int_{-\infty}^{\infty} Q(r,\theta,t)\,d\theta.$$

Integrating Eq. (26) over the phase θ, we get the equation of $P(r,t)$ as follows:

$$\frac{\partial P(r,t)}{\partial t} = -\frac{\partial}{\partial r}\{[(\lambda+\Gamma_{\rm eff})r-3r^3]P(r,t)\} + \frac{\partial^2}{\partial r^2}\left[\left(\frac{\bar{\varepsilon}}{2}+\Gamma_{\rm eff}r^2\right)P(r,t)\right] + \frac{\bar{\varepsilon}}{2r^2}\int_{-\infty}^{\infty}\frac{\partial^2 Q(r,\theta,t)}{\partial\theta^2}d\theta. \tag{28}$$

With a straightforward calculation for Eq. (28), the stationary probability density $P_{\rm st}(r)$ of $r(t)$ is obtained as

$$P_{\rm st}(r) = N\left(r^2+\frac{\bar{\varepsilon}}{2\Gamma_{\rm eff}}\right)^{(\eta-1)/2}\exp\left(-\frac{3}{2\Gamma_{\rm eff}}r^2\right)G(r). \tag{29}$$

Here, N is the normalization constant, and we defined

$$\eta = \frac{\lambda}{\Gamma_{\rm eff}}+\frac{3\bar{\varepsilon}}{2\Gamma_{\rm eff}}, \tag{30}$$

and

$$G(r) = -\int^{r}\left[\left(x^2+\frac{\bar{\varepsilon}}{2\Gamma_{\rm eff}}\right)^{-(\eta+1)/2}\exp\left(\frac{3}{2\Gamma_{\rm eff}}x^2\right)\times\int^{x}\left(\frac{\bar{\varepsilon}}{2y^2}\int_{-\infty}^{\infty}\frac{\partial^2 Q_{\rm st}(y,\theta)}{\partial\theta^2}d\theta\right)dy\right]dx, \tag{31}$$

where $Q_{\rm st}(r,\theta)$ is the steady state solution of Eq. (26). Since $l(t)\simeq\sqrt{2}r(t)$ because of $\hat{w}_n(t)\simeq 0$ except for n_c, the steady probability density $P(l)$ for $l(t)$ turns out to obey the asymptotic power law

$$P(l)\propto l^{-1+\eta}, \tag{32}$$

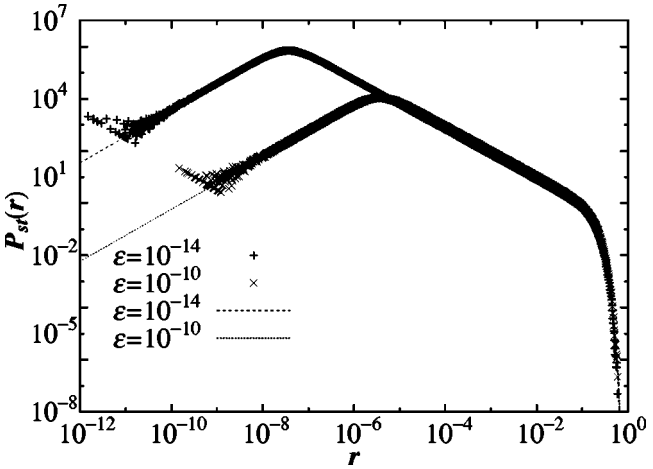

FIG. 11. Probability densities $P_{\rm st}(r)$ of the amplitude $r(t)$ of the k_c mode for parameter values same as in Figs. 7, 8, and 9. Shown are the results of numerical simulation with model *B* (symbols). The theoretical results are given by the lines. For details of the theory, see the text.

for small l if $\varepsilon=0$. However, it does not obey the asymptotic power law $l^{-1+\eta}$ in a small l region if $\varepsilon\neq 0$. These results agree with the simulation results as shown in Figs. 2 and 7.

We turn to the statistics of $\Delta\theta$. Suppose that $r(t)$ is constant since the characteristic time scale of $r(t)$ is much longer than that of $\theta(t)$, and that $\Delta\theta$ obeys the normal distribution with zero mean and variance $\bar{\varepsilon}\Delta t/r^2$ by Eq. (23). The probability density for the phase change for a given amplitude r is thus given by

$$p(\Delta\theta|r(t)=r) = \frac{r}{\sqrt{2\pi\bar{\varepsilon}\Delta t}}\exp\left[-\frac{r^2(\Delta\theta)^2}{2\bar{\varepsilon}\Delta t}\right]. \tag{33}$$

From Eq. (29), the stationary probability density $P(\Delta\theta)$ of $\Delta\theta$ is determined as

$$P(\Delta\theta) = \int_0^{\infty} p(\Delta\theta|r(t)=r)P_{\rm st}(r)\,dr = \frac{1}{\sqrt{\Delta t}}\phi\left(\frac{\Delta\theta}{\sqrt{\Delta t}}\right), \tag{34}$$

where

$$\phi(x) = \frac{N}{\sqrt{8\pi\bar{\varepsilon}}}\left(\frac{\bar{\varepsilon}}{2\Gamma_{\rm eff}}\right)^{(\eta+1)/2}\int_0^{\infty}(z+1)^{(\eta-1)/2}\times\exp[-z\psi(x)]G\left(\sqrt{\frac{\bar{\varepsilon}}{2\Gamma_{\rm eff}}z}\right)dz, \tag{35}$$

with the function $G(r)$ same as in Eq. (31), and we introduced

$$\psi(x) = \frac{3\bar{\varepsilon}}{4\Gamma_{\rm eff}^2}\left(1+\frac{\Gamma_{\rm eff}x^2}{\bar{\varepsilon}}\right). \tag{36}$$

Figure 11 shows the statistics of $r(t)$ numerically ob-

tained. In order to compare the theoretical result with numerical result, we assume

$$G(r)=\begin{cases} 1-\exp\left[-\left(\dfrac{2\Gamma_{\rm eff}}{\bar{\varepsilon}}r^2\right)^{1/2}\right] & (r\geqslant r_{\rm min}) \\ 0 & (r<r_{\rm min}), \end{cases} \tag{37}$$

where

$$r_{\rm min}=\delta^{-1}r_M, \quad r_M=\sqrt{\frac{\bar{\varepsilon}}{2\Gamma_{\rm eff}}}, \tag{38}$$

where δ is a certain constant which is phenomenologically introduced. In order to compare numerical result in Fig. 11, we put $\delta=10^4$. Hence, we obtain

$$\phi(x)=\frac{N}{\sqrt{8\pi\bar{\varepsilon}}}\left(\frac{\bar{\varepsilon}}{2\Gamma_{\rm eff}}\right)^{(\eta+1)/2}\int_{\delta^{-2}}^{\infty}\frac{1-\exp(-z^{1/2})}{(z+1)^{(1-\eta)/2}} \times\exp[-z\psi(x)]dz. \tag{39}$$

With the use of the asymptotic form

$$\frac{1-\exp(-z^{1/2})}{(z+1)^{(1-\eta)/2}}=\begin{cases} 2^{(\eta+3)/2}z^{1/2} & (z<1) \\ (z+1)^{(\eta-1)/2} & (z\geqslant 1). \end{cases}$$

$\phi(x)$ can be approximately obtained as

$$\begin{aligned}\phi(x)\approx&\frac{N}{\sqrt{2\pi\bar{\varepsilon}}}\left(\frac{\bar{\varepsilon}}{\Gamma_{\rm eff}}\right)^{(\eta+1)/2}\int_{\delta^{-2}}^{1}z^{1/2}\exp[-z\psi(x)]dz \\ &+\frac{N}{\sqrt{8\pi\bar{\varepsilon}}}\left(\frac{\bar{\varepsilon}}{2\Gamma_{\rm eff}}\right)^{(\eta+1)/2}\int_{1}^{\infty}(z+1)^{(\eta-1)/2} \times\exp[-z\psi(x)]dz \\ =&\frac{N}{\sqrt{2\pi\bar{\varepsilon}}}\left(\frac{\bar{\varepsilon}}{\Gamma_{\rm eff}}\right)^{(\eta+1)/2}[\psi(x)]^{-3/2}\left[\gamma\left(\frac{3}{2};\psi(x)\right)\right. \\ &\left.-\gamma\left(\frac{3}{2};\delta^{-2}\psi(x)\right)\right] \\ &+\frac{N}{\sqrt{8\pi\bar{\varepsilon}}}\left(\frac{\bar{\varepsilon}}{2\Gamma_{\rm eff}}\right)^{(\eta+1)/2}[\psi(x)]^{-(1+\eta)/2} \\ &\times\exp[\psi(x)]\Gamma\left(\frac{1}{2}(1+\eta);2\psi(x)\right),\end{aligned} \tag{40}$$

where $\gamma(z,p)$ and $\Gamma(z,p)$ stand for the first kind incomplete γ function and the second kind incomplete γ function, respectively. Furthermore, using the asymptotic forms [23,24],

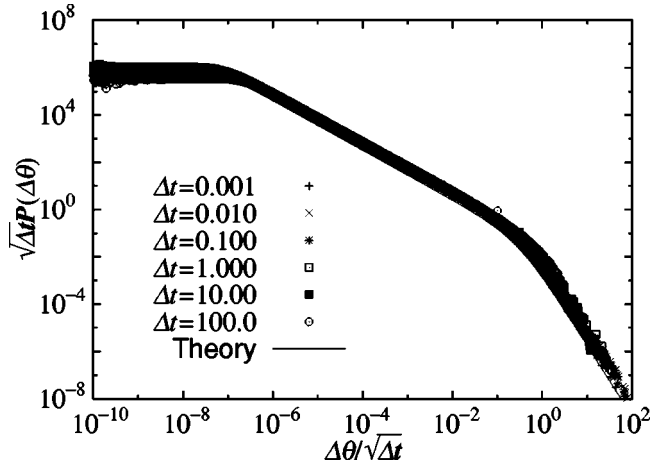

FIG. 12. Scaling forms of the probability densities $P(\Delta\theta)$ of $\Delta\theta(t)$ for $\lambda=0.002$, $D=100$, $\gamma=50$, and $\varepsilon=10^{-14}$. Shown are the results of numerical simulation for different values of Δt (symbols) in comparison with the theoretical result with Eq. (34) (line).

$$\gamma(z,p)\sim\begin{cases}0 & (p\ll z)\\ \Gamma(z) & (p\gg z),\end{cases}\quad \Gamma(z,p)\sim\begin{cases}\Gamma(z) & (p\ll z)\\ 0 & (p\gg z),\end{cases}$$

$$\begin{aligned}e^{p/2}\Gamma(z,p)=&p^{z-1}e^{-p/2} \\ &\times\left[1+\sum_{n=1}^{\infty}\frac{1}{p^n}(z-1)(z-2)\cdots(z-n)\right] \\ \sim&\begin{cases}\Gamma(z) & (p\to 0)\\ 0 & (p\to\infty),\end{cases}\end{aligned}$$

we obtain the asymptotic forms of Eq. (39) as follows:

$$\phi(x)\propto\begin{cases}\left(1+\dfrac{\Gamma_{\rm eff}}{3\bar{\varepsilon}}x^2\right)^{-(1+\eta)/2} & (x\ll\sqrt{2\Gamma_{\rm eff}}) \\ x^{-3} & (\sqrt{2\Gamma_{\rm eff}}\ll x\ll\delta\sqrt{2\Gamma_{\rm eff}}).\end{cases} \tag{41}$$

The theoretical result Eq. (39) is compared with the numerical simulation in Fig. 10 for $\varepsilon=10^{-14}$ and 10^{-10} with Δt being equal to the time step of the time integration. Theoretical results turn out to be in a good agreement with the results of numerical simulation. In addition, it should be noted that Eq. (41) also approximates the results of numerical simulation well. Here, since $\langle r^2\rangle\sim 10^{-3}$ estimated by using the result of numerical computation, Eq. (27) leads to $\Gamma_{\rm eff}\simeq\Gamma_f$. From Eq. (34), we have the scaling relation with the scaling function $\phi(x)$. Figure 12 depicts the scaling plot of the $P(\Delta\theta)$ for several different values of Δt, obtained from the numerical simulation with $\varepsilon=10^{-14}$. We find a good agreement between the theory and the simulation.

V. PHASE DIFFUSION ASSOCIATED WITH THE UNSTABLE MODE

Figure 13 shows the time series of $\theta(t)$ for the parameter values same as in Fig. 5. The temporal evolution of $\theta(t)$

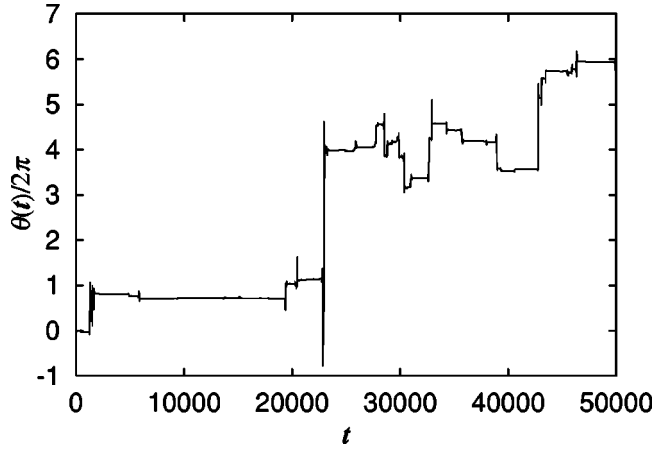

FIG. 13. Time series of the phase variable $\theta(t)$ of the k_c mode $\hat{w}_{n_c}(t)$ for the parameter values same as in Fig. 5.

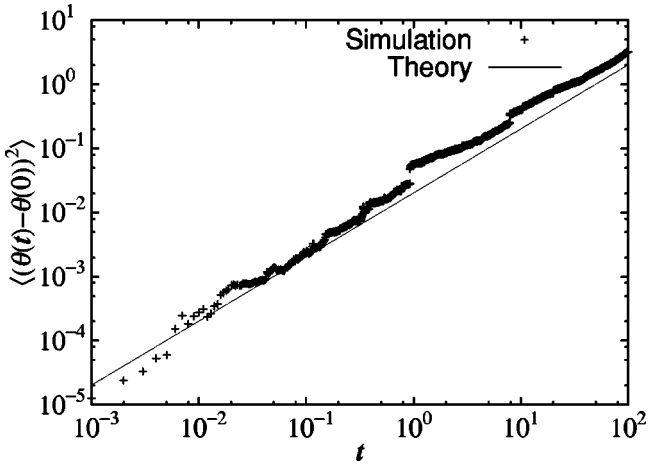

FIG. 14. Temporal evolution of the mean square displacement $\langle[\theta(t)-\theta(0)]^2\rangle$ plotted as a function of time difference t for $\lambda=0.002$, $D=100$, $\gamma=50$, and $\varepsilon=10^{-14}$. Shown are the results of numerical simulation (symbols) in comparison with the numerical integrations of Eqs. (29) and (37) (line).

shows apparently intermittent behaviors. By Eq. (23), we find that $\theta(t)$ changes considerably when $r(t)$ is small, i.e., when the state is in the laminar state. One expects that the phase variable shows a diffusive motion. In order to analyze the phase statistics, we study the mean square displacement $\langle[\theta(t)-\theta(0)]^2\rangle$ below. Since $g_\theta(t)$ is Gaussian-white noise which is independent of $g_r(t)$ and $r(t)$, the mean square displacement $\langle[\theta(t)-\theta(0)]^2\rangle$ is evaluated as

$$\langle[\theta(t)-\theta(0)]^2\rangle = 2D_{\rm diff}t, \tag{42}$$

for large t, where

$$D_{\rm diff}=\frac{\overline{\varepsilon}}{2}\left\langle\frac{1}{r^2(s)}\right\rangle=\frac{\overline{\varepsilon}}{2}\int_0^\infty r^{-2}P_{\rm st}(r)dr \tag{43}$$

is the phase diffusion constant. Figure 14 depicts the time-difference dependence of the mean square displacement $\langle[\theta(t)-\theta(0)]^2\rangle$ obtained by the numerical integration for the parameter values same as in Fig. 13. The numerical integrations of Eq. (43) carried out with the numerical integrations with Eqs. (29) and (37) is compared with the simulation in Fig. 14. Here, we again set $\delta=10^4$ and used the fact $\Gamma_{\rm eff}\simeq\Gamma_f$ since $\langle r^2\rangle$ is small. A good agreement between the theory and the numerical simulation is found. One should note that the present phase diffusion is generated by the presence of thermal noise.

In the time region when the amplitude $r(t)$ is large, thermal noise does not affect the phase change. On the other hand, when $r(t)$ is sufficiently small, thermal noise gives a considerable effect on the phase change. This is the origin of a global diffusive behavior of the phase, and therefore generates a considerable long-time change of convective pattern.

VI. CONCLUSION

In the present paper, we first introduced a phenomenological stochastic model of electrohydrodynamic convection in nematic liquid crystal under the external stochastic electric field. The model was organized as the Swift-Hohenberg equation with both spatially uniform external stochastic field and thermal noise. It was found that numerical simulation of the 1D system shows that a temporal evolution of the pattern intensity is intermittent and its statistics are same as three statistics of on-off intermittency so far known. These results explain JSB's experimental results. In the case when thermal noise is absent, we did not observe change of pattern form. On the other hand, when thermal noise is present, the temporally intermittent change of pattern form is observed. The temporal evolution of the phase of Fourier coefficient $\hat{w}_{n_c}(t)$ of the most unstable mode also changes simultaneously with intermittent pattern change. The intermittent change of convective pattern was in fact reported in a real experiment [14]. Since the phase of $\hat{w}_{n_c}(t)$ is directly related to the pattern itself, it is important to study the phase dynamics.

Moreover, in the present paper we studied the probability density $P(\Delta\theta)$ for the phase change $\Delta\theta(t)$ of the critical mode for an interval Δt, and found that the scaling relation (34) holds for a wide range of time steps Δt. Furthermore, we derived the asymptotic form of the scaling function [Eq. (41)]. It was found that in contrast to that the phase $\theta(t)$ of the k_c mode does not change when the amplitude $r(t)$ is large enough, it changes considerably due to thermal noise when the amplitude is small. Furthermore, it was shown that the phase variable shows a diffusion. We derived an approximate expression of the diffusion constant. Mean square displacement of phase theoretically obtained turned out to be in a good agreement with numerical simulation. Although a pattern change is obtained in laboratory experiment [14], no analysis of the pattern dynamics is carried out. We hope that analysis of the pattern dynamics in laboratory experiment is made and is compared with the present result in a near future.

Finally, although our model gives qualitatively same re-

sults as those experiments by John *et al.*, from the viewpoint of quantitative comparison of the present approach with the laboratory experiment, no direct correspondence of the parameters in our model to those in real experiments is known. We should further study to find concrete correspondence of the model parameters with those in experiments in future.

ACKNOWLEDGMENTS

H.F. thanks U. Behn, R. Stannariuss, and Th. John for informative discussions. The authors are also grateful to them for sending us the preprints of Refs. [13,14] prior to publication.

[1] H. Fujisaka and T. Yamada, Prog. Theor. Phys. **74**, 918 (1985); **75**, 1087 (1986).
[2] A. S. Pikovsky, Z. Phys. B: Condens. Matter **55**, 149 (1984).
[3] A. Pikovsky, M. Rosenblum, and J. Kurths, *Synchronization: A Universal Concept in Nonlinear Sciences* (Cambridge University Press, Cambridge, 2001).
[4] T. Yamada and H. Fujisaka, Prog. Theor. Phys. **76**, 582 (1986); H. Fujisaka and T. Yamada, *ibid.* **77**, 1045 (1987); **90**, 529 (1993); H. Suetani and T. Horita, Phys. Rev. E **60**, 422 (1999); H. Fujisaka, H. Suetani, and T. Watanabe, Prog. Theor. Phys. Suppl. **139**, 70 (2000); H. Fujisaka, S. Matsushita, and T. Yamada, J. Phys. A **30**, 5697 (1997); S. Miyazaki, J. Phys. Soc. Jpn. **69**, 2719 (2000).
[5] N. Platt, E. A. Spiegel, and C. Tresser, Phys. Rev. Lett. **70**, 279 (1993); J. F. Heagy, N. Platt, and S. M. Hammel, Phys. Rev. E **49**, 1140 (1994).
[6] T. Yamada, K. Fukushima, and T. Yazaki, Prog. Theor. Phys. Suppl. **99**, 120 (1989); E. Ott and J. C. Sommerer, Phys. Lett. A **188**, 39 (1994); Y. C. Lai and C. Grebogi, Phys. Rev. E **52**, R3313 (1995); A. Cenys, A. Tamserius, and T. Schneider, Phys. Lett. A **213**, 259 (1996); S. C. Venkataramani, T. M. Antonsen, Jr., E. Ott, and J. C. Sommerer, Physica D **96**, 66 (1996); Y. C. Lai, Phys. Rev. E **53**, R4267 (1996); **54**, 321 (1996); T. Harada, H. Hata, and H. Fujisaka, J. Phys. A **32**, 1557 (1999).
[7] F. Rödelsperger, A. Cenys, and H. Benner, Phys. Rev. Lett. **75**, 2594 (1995); H. Fujisaka, K. Ouchi, H. Hata, B. Masaoka, and S. Miyazaki, Physica D **114**, 237 (1998); J. Becker, F. Rödelsperger, Th. Weyrauch, H. Benner, W. Just, and A. Cenys, Phys. Rev. E **59**, 1622 (1999).
[8] M. C. Cross and P. C. Hohenberg, Rev. Mod. Phys. **65**, 851 (1993).
[9] *Pattern Formation in Liquid Crystals*, edited by A. Buka and L. Kramer (Springer-Verlag, Berlin, 1996).
[10] S. Kai, T. Kai, M. Tanaka, and K. Hirakawa, J. Phys. Soc. Jpn. **47**, 1379 (1979); T. Kawakubo, A. Yanagita, and S. Kabashima, *ibid.* **50**, 1451 (1981); H. R. Brand, S. Kai, and S. Wakabayashi, Phys. Rev. Lett. **54**, 555 (1985); S. Kai, H. Fukunaga, and H. R. Brand, J. Phys. Soc. Jpn. **56**, 3759 (1987); J. Stat. Phys. **54**, 1133 (1987).
[11] U. Behn, A. Lange, and T. John, Phys. Rev. E **58**, 2047 (1998).
[12] T. John, R. Stannarius, and U. Behn, Phys. Rev. Lett. **83**, 749 (1999).
[13] U. Behn, T. John, and R. Stannarius, in *Experimental Chaos*, edited by Stefano Boccaletti, Bruce J. Gluckman, Jürgen Kurths, Louis M. Pecora, and Mark L. Spano, AIP Conf. Proc. No. 622 (AIP, Melville, NY, 2002).
[14] T. John, U. Behn, and R. Stannarius, Phys. Rev. E **65**, 046229 (2002).
[15] H. Fujisaka, K. Ouchi, and H. Ohara, Phys. Rev. E **64**, 036201 (2001).
[16] J. Swift and P. C. Hohenberg, Phys. Rev. A **15**, 319 (1977).
[17] P. Manneville, *Dissipative Structures and Weak Turbulence* (Academic, New York, 1990).
[18] J. G-Ojalvo and J. M. Sancho, *Noise in Spatially Extended Systems* (Springer-Verlag, Berlin, 1999).
[19] P. E. Kloeden, E. Platen, and H. Schurz, *Numerical Solution of SDE Through Computer Experiments* (Springer-Verlag, Berlin, 1997).
[20] X. Luo and S. Zhu, Eur. Phys. J. D **19**, 111 (2002).
[21] *Noise in Nonlinear Dynamical Systems*, edited by F. Moss and P. V. E. McClontoc (Cambridge University Press, Cambridge, 1989), Vols. 1–3.
[22] H. Risken, *The Fokker-Planck Equation* (Springer-Verlag, Berlin, 1984).
[23] *Handbook of Mathematical Functions*, edited by M. Abramowitz and I. A. Stegun (Dover, New York, 1965).
[24] W. H. Press, B. P. Flannery, S. A. Teukolsky, and W. T. Vetterling, *Numerical Recipes in C* (Cambridge University Press, Cambridge, 1988).